PROPELLER FLOW VISUALIZATION TECHNIQUES

George L. Stefko, F. J. Paulovich, J. P. Greissing and E. D. Walker

NASA Lewis Research Center

Cleveland, Ohio

ADVANCED PROPELLER IN LEWIS 8 × 6 WIND TUNNEL

Advanced propeller designs for future fuel-efficient high-subsonic speed aircraft are being investigated in the Lewis 8 × 6 wind tunnel to determine their performance, noise, and aeroelastic characteristics. These advanced propeller designs have thin, highly swept blade shapes which can experience large structural deflections under the operating loads of high-speed flight. These blade deflections may significantly alter the propeller operating characteristics. To investigate this important area, new propeller stroboscopic measurement techniques have been developed. With these techniques, the flutter motion and blade deflected shape of a rotating propeller can be determined. In addition, tuft, oil, and paint flow visualization of the local blade flow field can be accomplished.

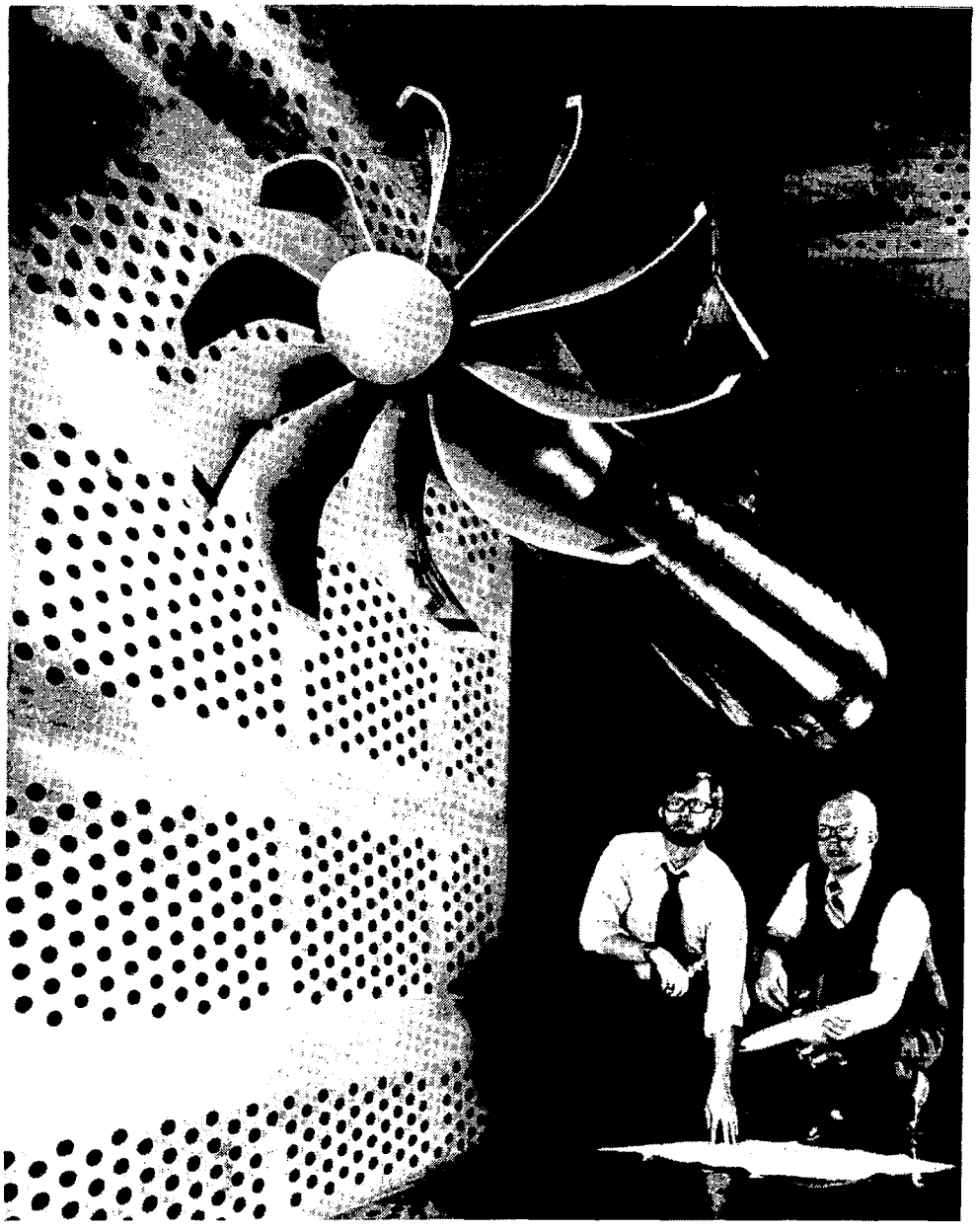

PROPELLER FLOW VISUALIZATION

Two propeller stroboscopic measurement systems were developed to perform propeller flow visualization work on advanced propellers in the Lewis wind tunnels. One propeller measurement system used a video photographic system while the other used a 35-mm photographic system.

The video stroboscopic photographic system was used to record: (1) propeller flutter blade motions, (2) blade-to-blade differences in blade tip motion, and (3) the on-line television pictures to position the propeller for the 35-mm photographs.

The 35-mm stroboscopic photographic system was used to record: (1) propeller blade tip deflections under steady centrifugal and aerodynamic loads, (2) tuft patterns on the rotating propeller blade, and (3) surface flow patterns on the propeller blades including a new "paint flow" technique.

- EQUIPMENT
- FLUTTER MOTION
- BLADE TIP DEFLECTION
- TUFTS
- PAINT FLOW

ELECTRONIC CONTROL DIAGRAM

This diagram illustrates the major pieces of equipment in the two photographic systems developed to take pictures of propellers in the wind tunnel at rotation speeds up to 10 000 revolutions per minute (RPM). The propeller's once-per-revolution signal is delayed by an Angle Encoder so that the propeller blades can be viewed in any desired angular position. The modified once-per-revolution signal is then sent to the Dual Strobe controller which allows one to take video or 35-mm pictures.

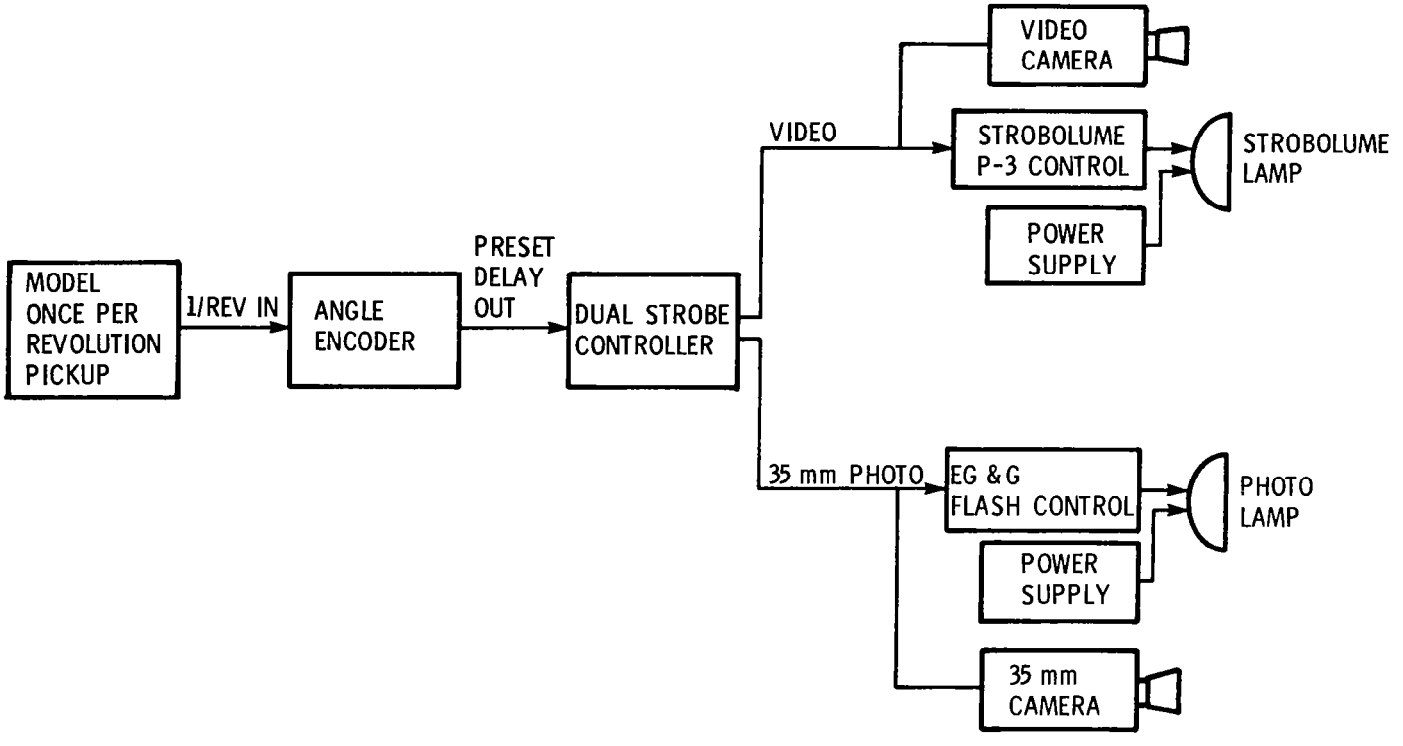

ELECTRONIC CONTROLLERS

The Angle Encoder controller and the Dual Strobe controller are shown in this figure. The Angle Encoder allowed the propeller blades to be positioned in any desired rotational position within 0.01°. The Dual Strobe controller allowed the pictures to be taken remotely from the wind tunnel control room.

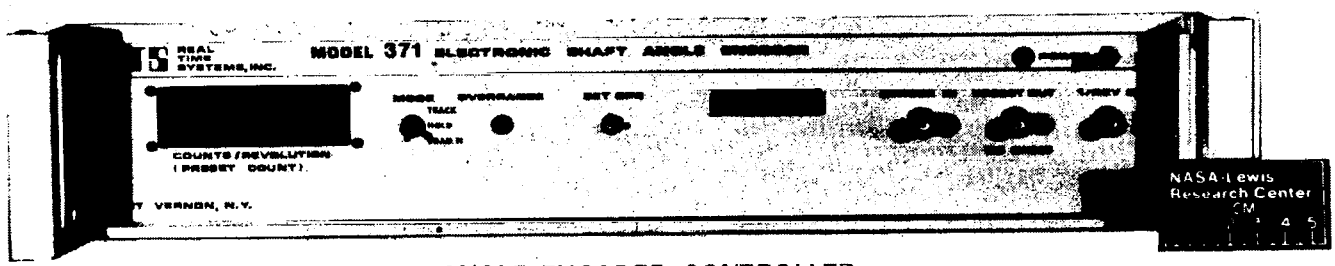

ANGLE ENCODER CONTROLLER

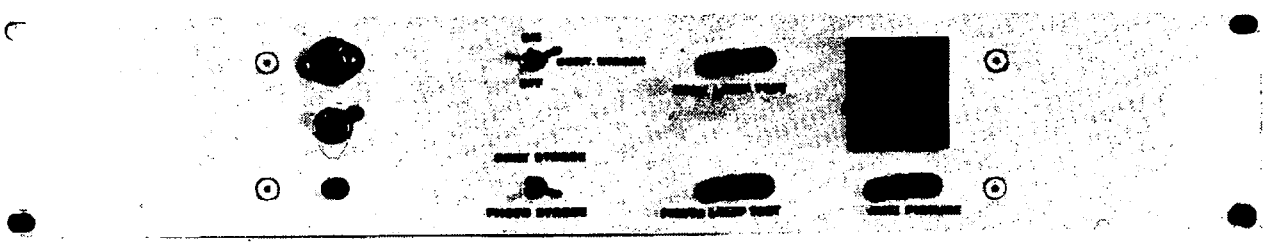

DUAL STROBE CONTROLLER

VIDEO PHOTOGRAPHIC SYSTEM

The video stroboscopic photographic system consisted of a Sony video camera (AVC-1400), a General Radio stroboscope (Strobolume 1540), a Sony videocassette recorder (Betamax SL-5400) and a television. Pictures of the hardware are shown in the figure.

The camera was positioned 5 ft from the propeller centerline while the flash head was positioned 3 ft from the propeller centerline. The videocassette recorder and television monitor were located in the wind tunnel control room.

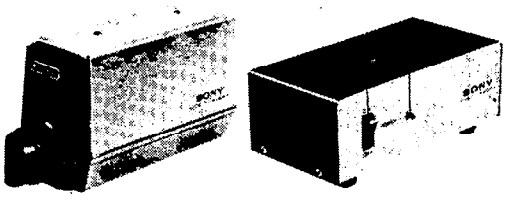

SONY VIDEO CAMERA

SONY VIDEO RECORDER

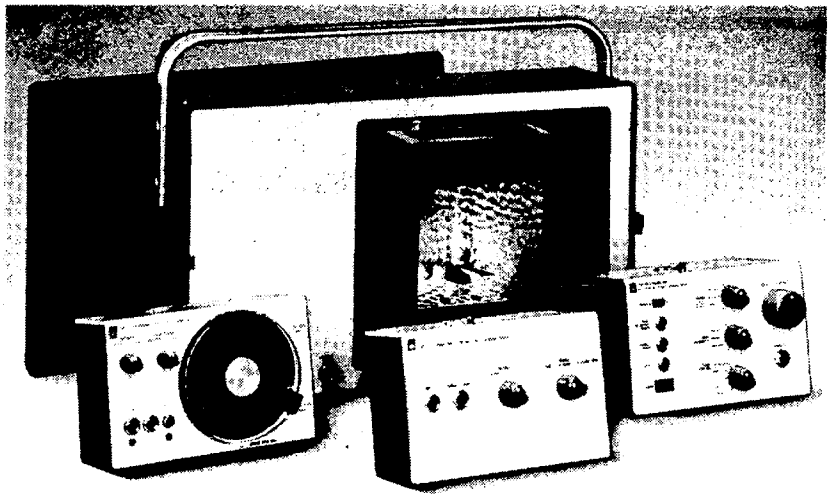

GR VIDEO STROBOSCOPE

35-mm PHOTOGRAPHIC SYSTEM

The 35-mm stroboscopic photographic system consisted of an Olympus 35-mm camera (OM-1) and an EG&G stroboscope (549 microflash). Pictures of this hardware are shown in this figure.

The best combination of camera variables were as follows: (1) an 85-mm lens, (2) an f-stop of 4.0, (3) an ASA 400 film processed at the equivalent speed of ASA 1200 film, (4) a 1 μsec (1×10^{-6} sec) stroboscope flash duration, (5) a stroboscope flash head positioned 3 ft from the propeller centerline, and (6) a camera positioned 5 ft from the propeller centerline.

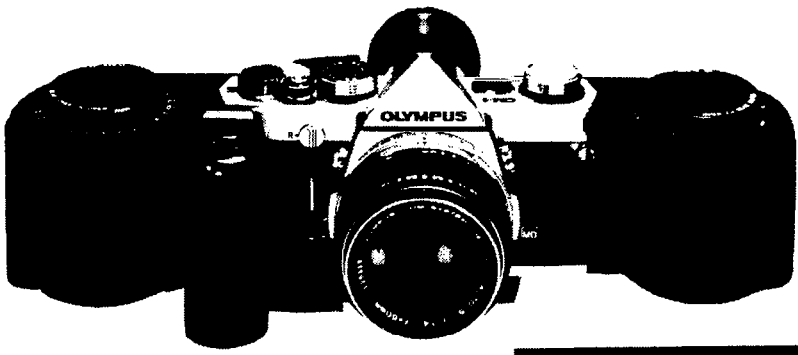

OLYMPUS CAMERA

EG & G STROBOSCOPE

FLUTTER MOTION OF THE SR-5 PROPELLER

This figure shows the blade flutter that occured with the SR-5 propeller model (i.e., 24 in. diameter) in the Lewis 8 × 6 wind tunnel. The video system recorded each blade in flutter so that the blade to blade variations in the vibration amplitude could be assessed. Also, the video recordings allowed the approximate shape of the blade motion to be assessed.

These video recordings were very useful in understanding the nature of the flutter instability. It was determined that the flutter was a coupled bending-torsion type of flutter and that the following factors were significant in causing the flutter: (1) high blade sweep, (2) cascade effect, and (3) compressibility. With this knowledge, analytical methods were developed to predict the flutter.

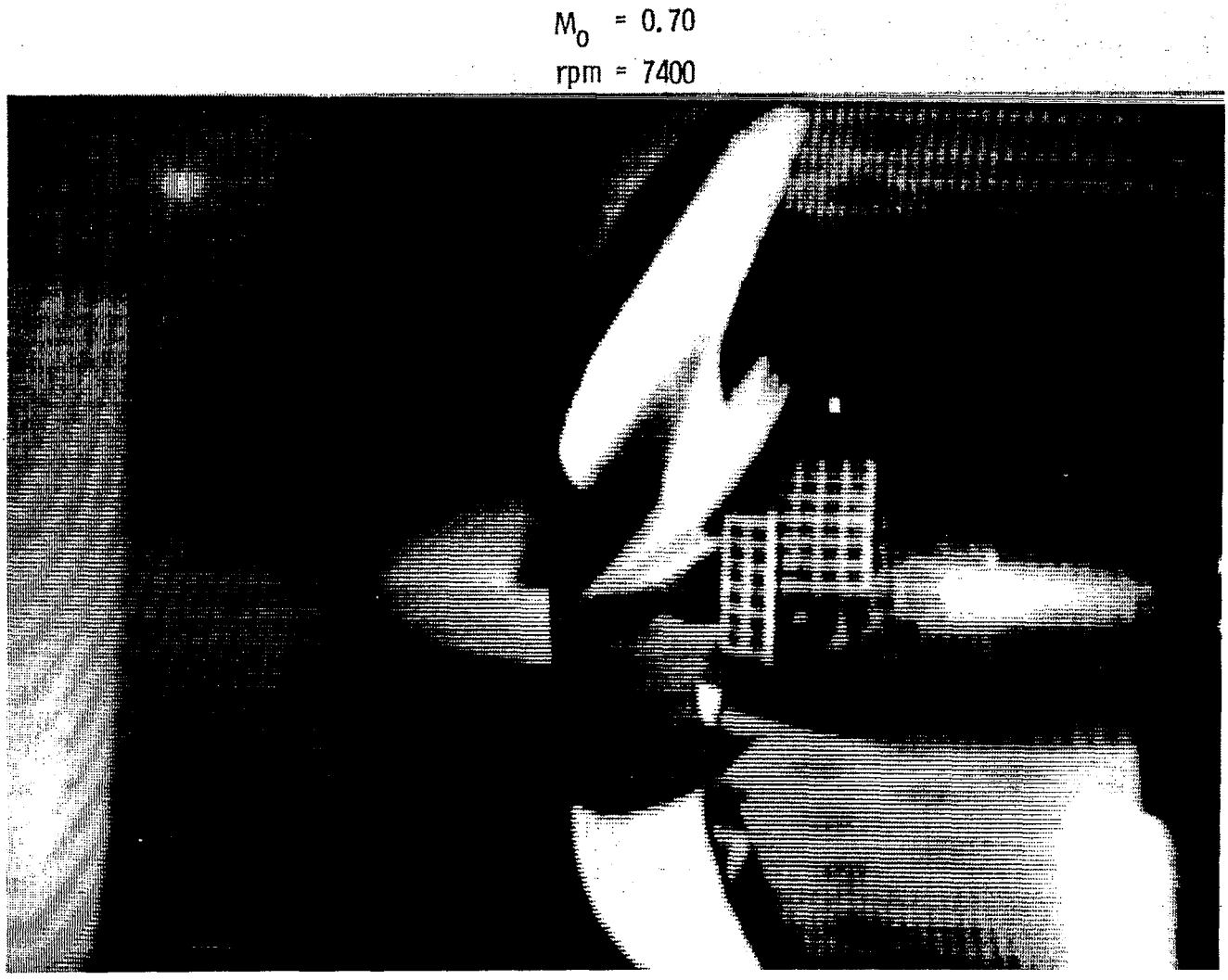

SR-5 CLASSICAL FLUTTER SUMMARY

The conditions where three SR-5 propeller configurations were in the coupled bending-torsion flutter are plotted in terms of the propeller RPM, tunnel Mach number, and number of blades on the propeller. The number of blades on the SR-5 propeller hub was varied from two to five to ten blades to determine the blade cascade effect on the flutter. The larger number of blades caused the onset of flutter to occur earlier (i.e., at lower Mach numbers and RPM). This experimentally demonstrated that the blade aerodynamic cascade effects have an unfavorable effect on flutter. The places where video recordings were made of the flutter motion are indicated by the solid triangular symbols.

Two flutter boundaries are indicated by the cross-hatched lines. Two different flutter prediction methods were used to predict these boundaries as follows: (1) a modal analysis with plate modes in conjunction with two dimensional (2D) subsonic single blade unsteady aerodynamic theory, and (2) a beam model with 2D subsonic unsteady cascade aerodynamic theory. It can be seen that the flutter boundary predicted by the beam model is in better agreement with the measured data primarily because it accounted for cascade effects.

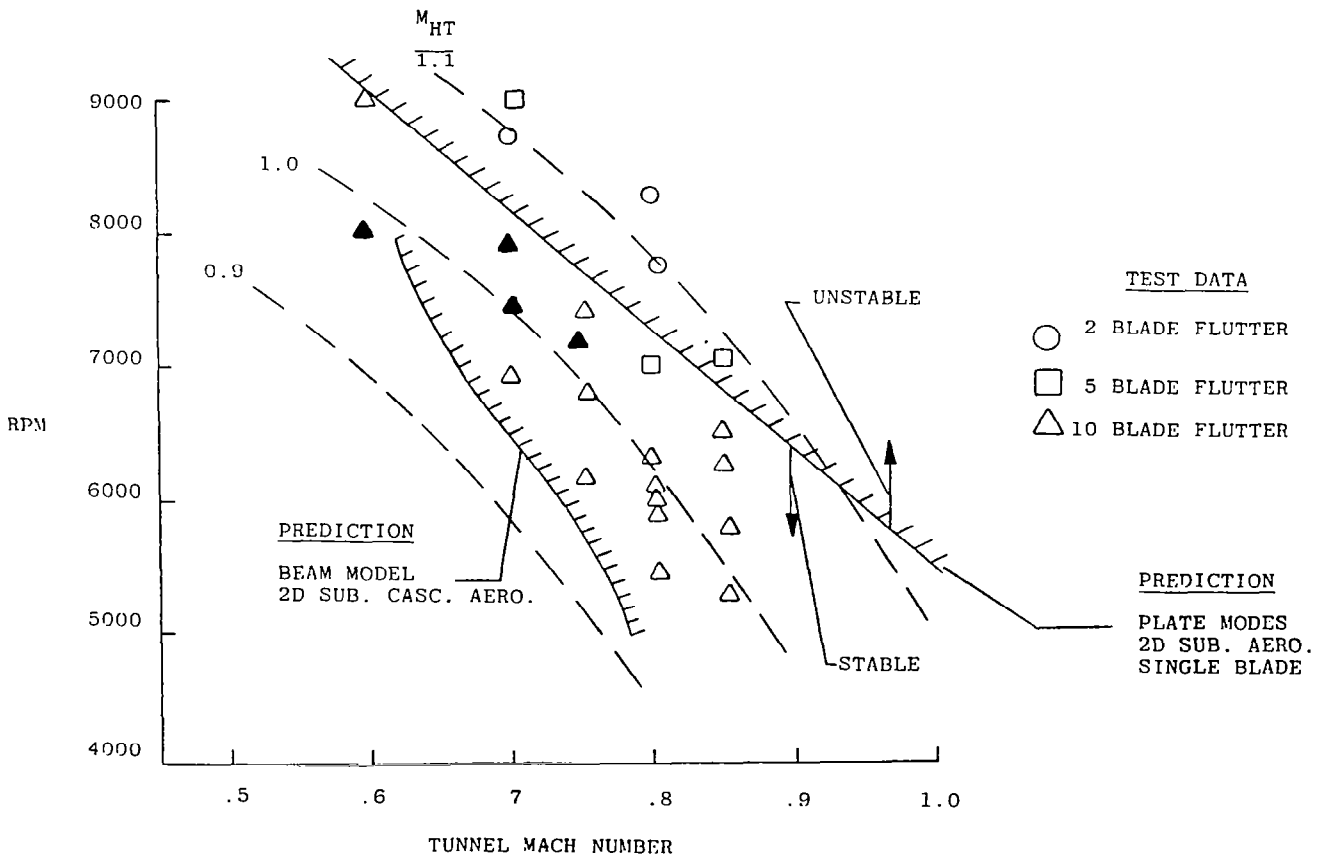

PROPELLER BLADE TIP DEFLECTION MEASUREMENT TECHNIQUE

It is very important to know the actual operating propeller blade shape as it determines the actual propeller performance and noise. Therefore, propeller blade tip movement under steady centrifugal and aerodynamic loading were measured using the 35-mm stroboscopic photographic system. In this figure, two photographs are shown of the SR-5 propeller (that incorporated 60° of tip sweep) operating at a blade angle of 59° ($\beta_{3/4}$ = 59°). The photograph on the left side was taken as the wind tunnel started running with the propeller at 750 RPM and the tunnel at a Mach number of approximately 0.10. The photograph on the right side illustrates the propeller at a rotational speed of 9000 RPM and a tunnel Mach number of 0.45. The blade tip deflections were determined by measuring displacements relative to the aligned grid pattern on the rotating hub and static nacelle. These initial results demonstrated the ability to photographically determine the advanced propeller blade steady state tip deflections. These blade tip deflections are compared with analytical predictions in the next figure.

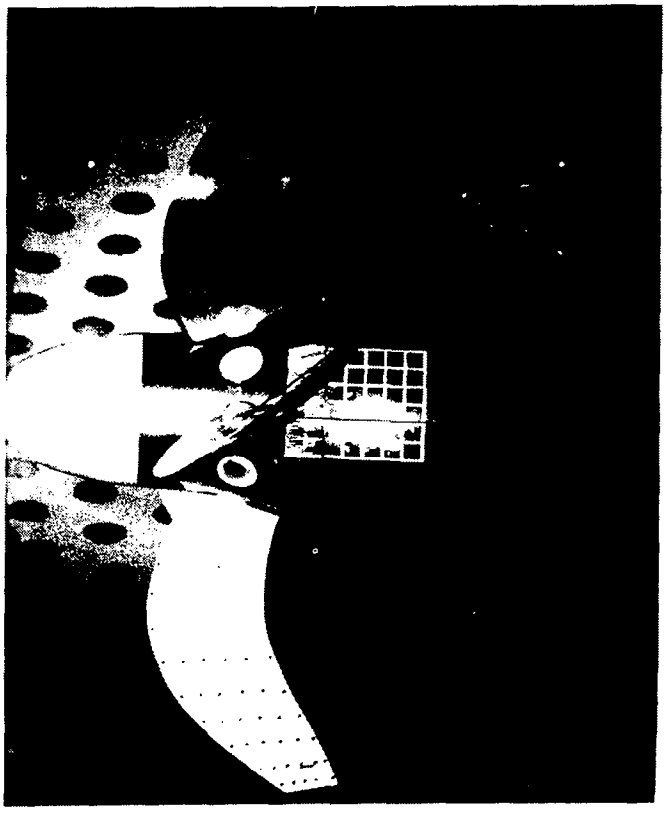

rpm = 750
$M_o \sim 0.1$

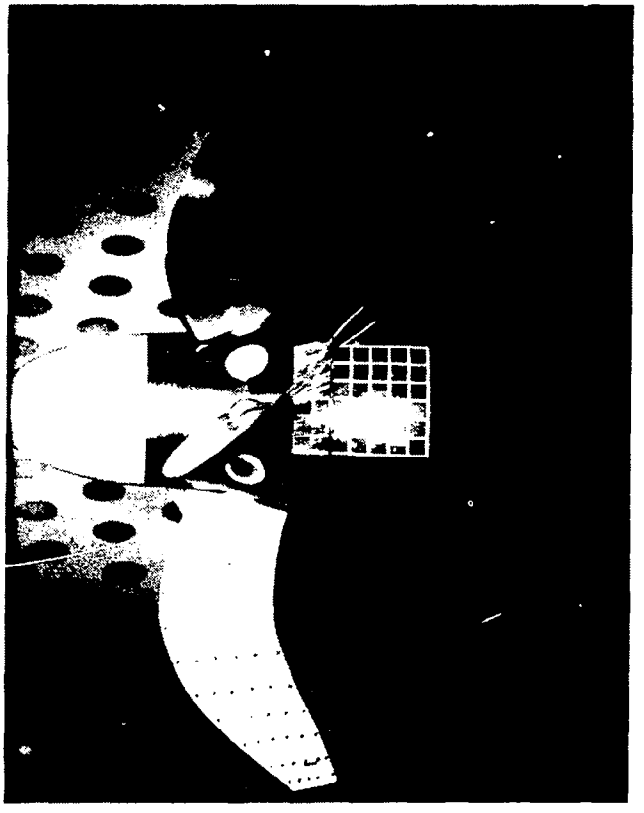

rpm = 9000
M_o = 0.45

SR-5 BLADE TIP MOVEMENT

A comparison of the measured blade tip twist with finite element structural prediction methods is shown in this figure. At rotational speeds near 8000 RPM, the data shows that the structural prediction methods underestimated the blade twist about 1.5° to 4.0°. The figure also shows that as the propeller rotational speed was increased to 9000 RPM, the blade twist reached 9.5°. With the blade twisting to 9.5°, the blade tip trailing edge moved about 0.4 in. horizontally and 0.5 in. vertically. The sketch at the top of the figure shows the approximate positions of the blade tip at rotational speeds of 750 and 9000 RPM.

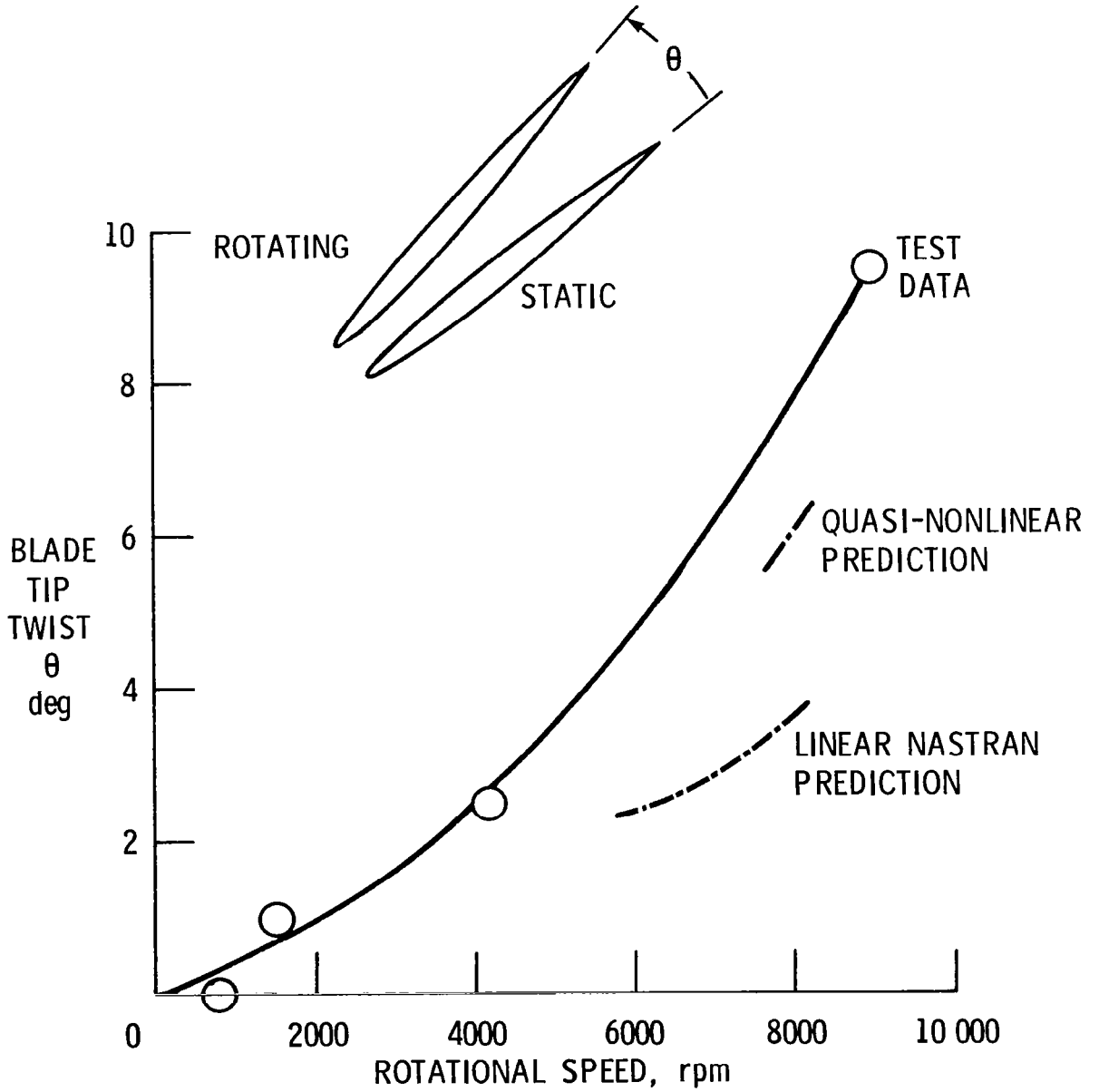

TUFT FLOW VISUALIZATION TECHNIQUE

Tufts with a diameter of 0.007 were installed on the propeller blades. The tuft flow patterns due to aerodynamic and centrifugal forces are shown for the SR-5 propeller operating at 0.75 free-stream Mach number, 7200 RPM, and a blade angle of 64° (i.e., $\beta_{3/4} = 64°$). The tufts radial alignment, especially near the blade tip, indicates that the centrifugal force on the tufts dominated the aerodynamic force. Consequently, the flow directions are more typical of the boundary layer flow directions than the free-stream aerodynamic flow directions over the blade. Further, at the conditions the tufts were tested, no stall regions were evident on the propeller blades.

$M_0 = 0.75$
rpm = 7200

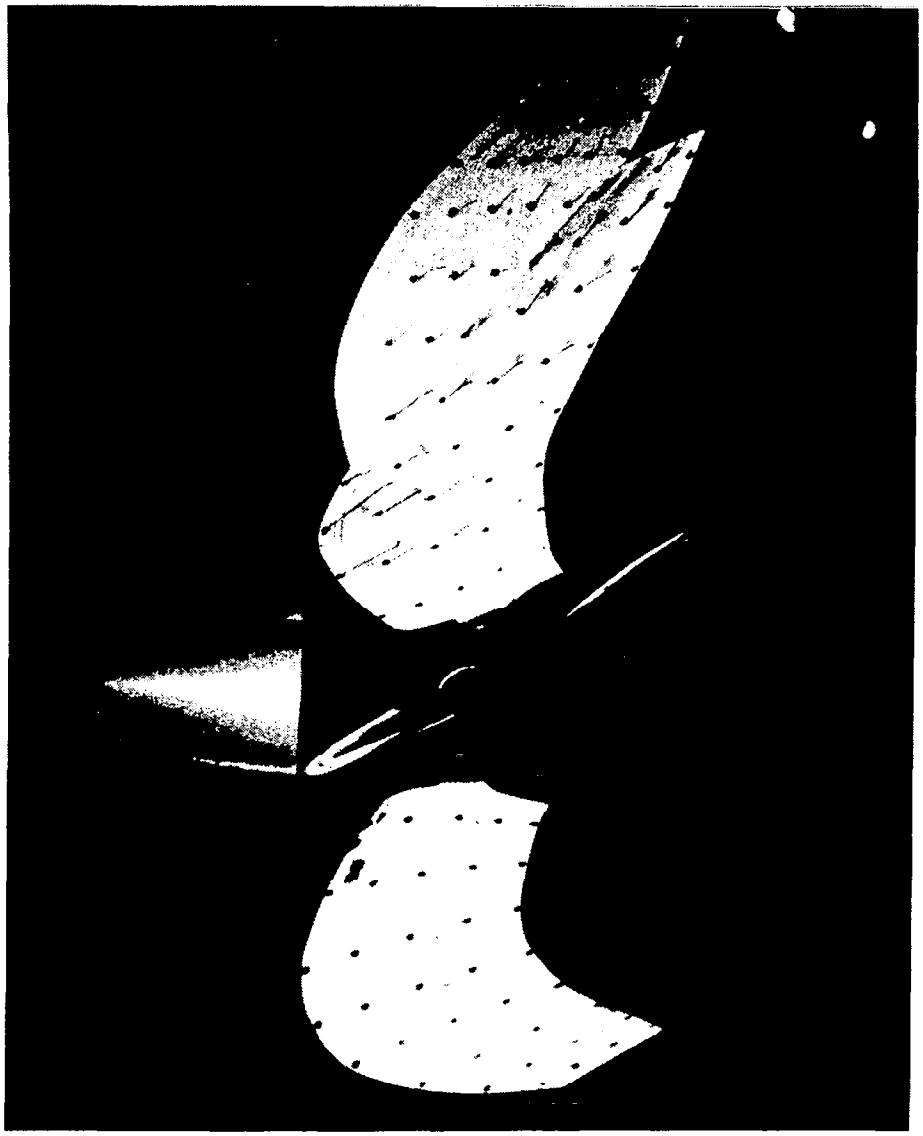

COMPARISON OF 8 AND 10 BLADE PERFORMANCE

This figure shows the ten-blade SR-6 propeller performance loss due to shock waves in the root region. The propeller net efficiency for the ten-blade SR-6 and the eight-blade SR-3 propellers are presented versus free-stream Mach number for an advance ratio of 3.5 and a power coefficient of 2.03. The SR-6 ten-blade propeller indicates a rapid drop in efficiency for Mach numbers above 0.77. Although a couple of hypotheses for the efficiency loss existed previously, the paint flow test established blade root choking as the most probable cause of the propeller performance loss.

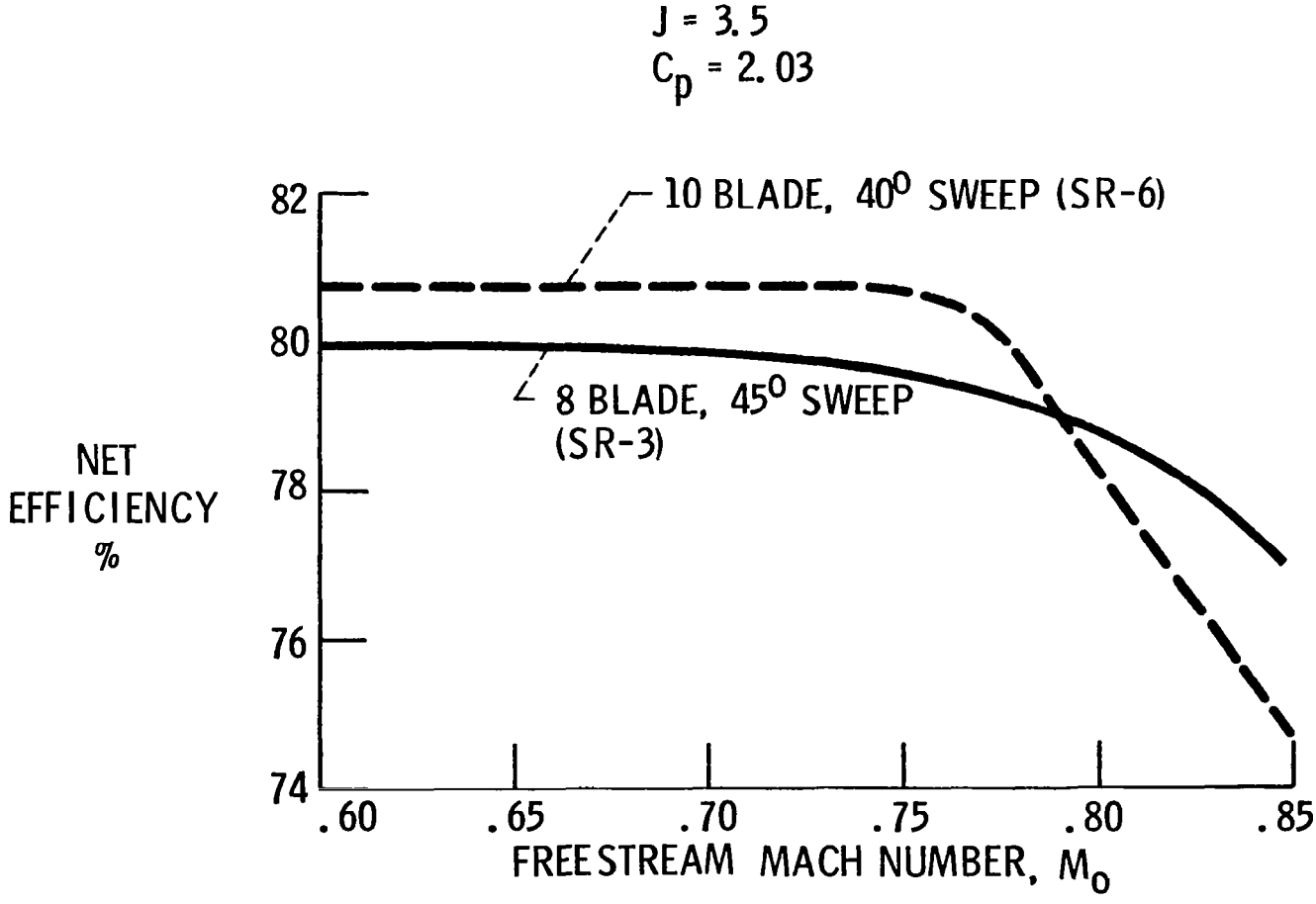

SHOCK WAVE LOCATIONS ON THE SR-6 PROPELLER BLADES

The paint flow technique was used on the ten-blade SR-6 propeller to determine if it could locate shock waves. The propeller was tested at a free-stream Mach number of 0.80, a rotational speed of 8000 RPM, a blade angle of 58°, an advanced ratio of 2.85, and a power coefficient of 1.35. The technique worked well. It showed shock waves located between the propeller blades which were especially strong in the blade root region. The figure shows the actual shock wave pattern on the propeller blades. Note the discontinuous change in flow direction behind the shock wave which is more clearly evident in the picture on the left side.

These shock waves show that the flow was choked in the propeller root regions. This flow choking gave rise to the shock waves which cause a loss of propeller efficiency at the higher Mach numbers.

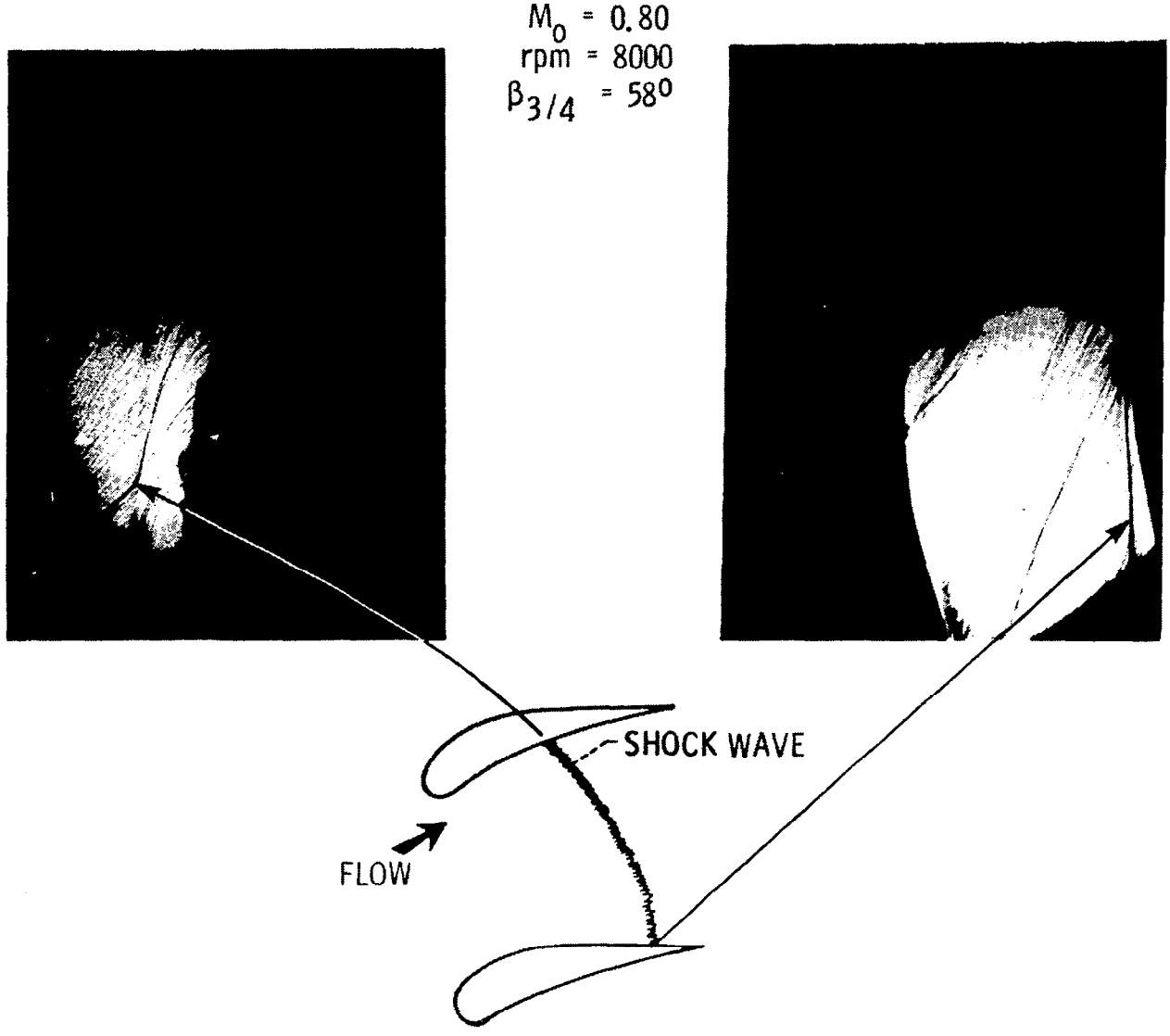

RESULTS

It is very important to know the actual operating blade shape as it determines the actual propeller performance and noise. These results demonstrated the ability to photographically determine the advanced propeller blade tip deflections, local flow field conditions, and gain insight into aeroelastic instability.

With this new knowledge, the analytical prediction methods that are under development can be compared with experimental data. These comparisons will contribute to the verification of these improved methods and will give improved capability for designing future advanced propellers with enhanced performance and noise characteristics.

- TWO PROPELLER PHOTOGRAPHIC SYSTEMS WERE DEVELOPED
- FLUTTER MOVIES DETERMINED TYPE OF FLUTTER
- BLADE TIP DEFLECTIONS WERE MEASURED
- TUFTS SHOWED NO STALL REGIONS
- PAINT FLOW TECHNIQUE SHOWED SHOCK WAVES